

# Carbon Nanomembranes from Aromatic Carboxylate Precursors

Petr Dementyev,<sup>\*[a]</sup> Daniil Naberezhnyi,<sup>[a]</sup> Michael Westphal,<sup>[a]</sup> Manfred Buck,<sup>\*[b]</sup> and Armin Götzhäuser<sup>[a]</sup>

Self-assembled monolayers (SAMs) serve as convenient platform for fabricating carbon nanomembranes (CNMs) of extended lateral dimensions. Highly porous CNMs are emerging as interesting materials for membrane technologies as they exhibit selectivity for water permeation and, owing to their reduced dimensionality, promise increased energy efficiency compared to established systems. In the present study terphenylcarboxylate SAMs, prepared on silver underpotential deposited on Au and irradiated by 100 eV electrons, were successfully converted into free-standing CNMs. Infrared and X-ray photoelectron

spectroscopy reveal pronounced chemical changes both of the anchoring carboxylate moiety and the aromatic backbone upon electron irradiation. Permeation studies showed high specificity for water as demonstrated by the separation from tetrahydrofuran. Compared to thiols on gold, the standard CNM precursor system, the carboxylic acid based SAM exhibits equivalent characteristics. This suggests that electron-induced carbonization is insensitive to the particular choice of the anchor moiety and, therefore, the choice of precursor molecules can be extended to the versatile class of aromatic carboxylic acids.

## 1. Introduction

With membrane separation gaining increasing technological importance, designing well-defined pores and narrowing their size distribution as well as minimizing the thickness of active layers are among the main strategies to advance the respective processes.<sup>[1]</sup> In this regard, a few classes of nanostructured membranes, such as metal-organic frameworks (MOFs),<sup>[2]</sup> covalent-organic frameworks (COFs),<sup>[3]</sup> zeolites,<sup>[4]</sup> and carbonaceous materials,<sup>[5]</sup> have demonstrated an intriguing potential, even though industrial readiness has not yet been reached. Graphitic and amorphous carbon is particularly advantageous due to its thermal and chemical stability, ease of fabrication, and low costs. However, pyrolytic carbon often exhibits significant fragility when prepared on a thickness scale of several micrometers. In contrast, nanometer-thick carbon nanomembranes (CNMs) made from self-assembled monolayers (SAMs) via electron bombardment are flexible and have outstanding mechanical characteristics.<sup>[6]</sup> Since SAMs are formed upon adsorption of organic molecules on solid surfaces, there is no principal limitation on the size of CNMs produced, and


continuous films have been studied under both supported and free-standing conditions.<sup>[6]</sup>

As a rule, SAMs represent highly ordered structures whose properties are prescribed by the nature of their molecular precursors and the underlying substrates.<sup>[7]</sup> The chemical interactions between the surface and the adsorbates are determined by the head groups, while the molecular backbones govern the macroscopic behavior of the layers, including electronic and optical phenomena. The electron-induced synthesis of CNMs has typically been done on gold substrates and cross-linking of the SAM molecules was proven to occur with different polyaromatic thiols.<sup>[8]</sup> The influence of the precursor molecules has been established for diverse extensive properties, such as mechanical strength and electrical conductivity.<sup>[9]</sup> However, the microstructure of the final material remained rather elusive, despite numerous spectroscopic efforts to understand the mechanism of the radiation carbonization.<sup>[10]</sup> Recently, Neumann *et al.* have pioneered CNMs prepared from SAMs of aromatic carboxylic acids on silver substrates, suggesting that the scope of this nanofabrication method can be significantly widened by this type of compounds.<sup>[11]</sup> Indeed, compared to thiols which are prone to oxidation under ambient conditions and require delicate handling upon functionalization and use,<sup>[12]</sup> aromatic carboxylic acids are more benign from the synthesis point of view and the large variety of commercially available precursor molecules would be highly beneficial, provided material performance is not compromised.

Thus far, terphenylthiol (TPT) (Figure 1) has been mostly employed as a precursor in mass transfer experiments with free-standing CNMs.<sup>[13,14]</sup> In particular, TPT CNMs were found to enable selective permeation of water molecules in mixtures with a range of gases and organic vapors.<sup>[15–17]</sup> The topography of the material was probed with atomic force microscopy (AFM), and densely packed arrays of ordered TPT molecules were revealed to be transformed completely to a new sponge-

[a] Dr. P. Dementyev, D. Naberezhnyi, M. Westphal, Prof. Dr. A. Götzhäuser  
Physics of Supramolecular Systems and Surfaces  
Bielefeld University  
Universitätsstr. 25, 33615 Bielefeld (Germany)  
E-mail: dementyev@physik.uni-bielefeld.de

[b] Prof. Dr. M. Buck  
EaStCHEM School of Chemistry  
University of St Andrews  
North Haugh, St Andrews KY16 9ST (U.K.)  
E-mail: mb45@st-andrews.ac.uk

 © 2020 The Authors. Published by Wiley-VCH Verlag GmbH & Co. KGaA. This is an open access article under the terms of the Creative Commons Attribution Non-Commercial License, which permits use, distribution and reproduction in any medium, provided the original work is properly cited and is not used for commercial purposes.

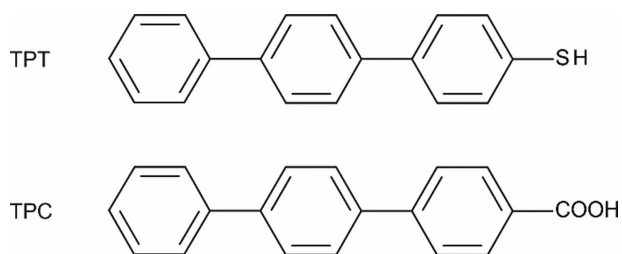


**Figure 1.** Molecular structures of TPT and TPC precursors.

like morphology. In this study, we advance CNM preparation using gold substrates modified by underpotential deposition (UPD) of a bilayer of silver, in order to impart affinity for carboxylic acids. The UPD-Ag substrates were exposed to terphenyl carboxylic acid (TPC) (Figure 1) to form SAMs, followed by electron irradiation to produce CNMs. The synthesis process was characterized by scanning tunneling microscopy (STM), helium ion microscopy (HIM), infrared reflection absorption spectroscopy (IRRAS), and X-ray photoelectron spectroscopy (XPS). Finally, comparative experiments on molecular permeation were carried out to explore whether the micro-porous structure of CNMs is affected by the change of the head group.

## 2. Results and Discussion

### 2.1. Structural Characterization

Self-assembly of TPC molecules on electrodeposited silver was studied previously.<sup>[18]</sup> Anchored to the substrate by coordination bonding of the carboxylate moiety, the molecules stand upright and form a highly crystalline single-phase overlayer (Figure 2a,b). The lattice is described by a rectangular ( $5 \times \sqrt{3}$ ) unit cell, and the packing density corresponds to 4.17 molecules/nm<sup>2</sup>. It is noticed that the appearance of the structure is sensitive to the tunneling conditions. Depending on the condition of the tip, not all molecules might be resolved as illustrated by the comparison of Figures 2a and 2b. In the image of Figure 2a, the protrusions reflect only a subset of the molecules which would suggest a much lower packing density. That this is not the true structure is evidenced by the image of Figure 2b where a change in contrast occurs during the scan. The structure in the central part of the image looks like the one in Figure 2a, as indicated by the yellow unit cell, whereas the top part shows additional protrusions and the unit cell as described previously.<sup>[18]</sup>

Different from TPC, TPT interacts with the gold surface through covalent Au–S bonds and exhibits polymorphous periodicity.<sup>[19]</sup> Despite the fact that the phases differ by 10–20° in the tilt angle, TPT SAMs are characterized by an average areal density of 3.82 molecules/nm<sup>2</sup>, which is, within less than 10% difference, comparable to TPC SAMs. At the same irradiation dose employed for the thiol, TPC SAMs are readily converted into CNMs. Figure 2c shows a free-standing CNM made from

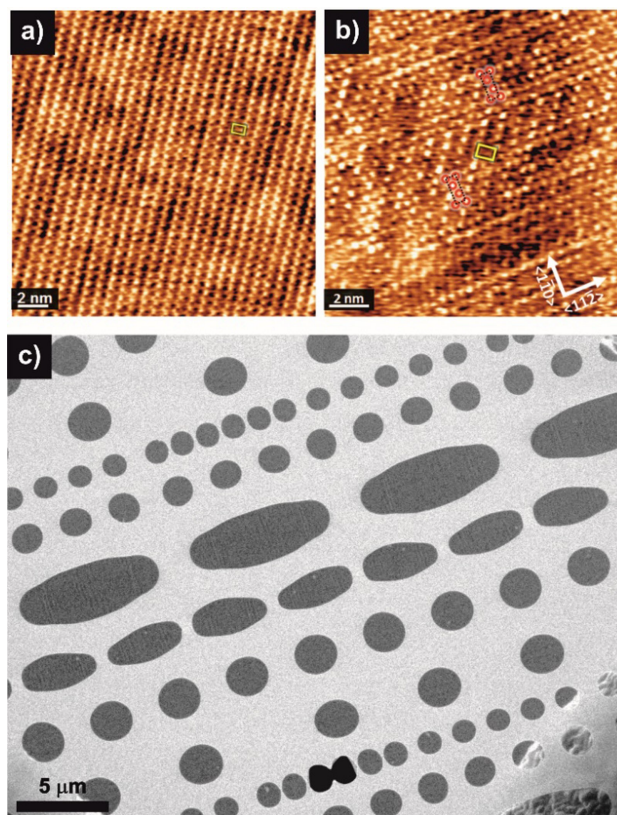


**Figure 2.** a,b) Molecularly resolved STM images of TPC SAM on Ag/Au/mica at different magnification. The ( $5 \times \sqrt{3}$ ) unit cell and the packing of the molecules are indicated in (b) by the black dotted rectangles and the red circles, respectively. The unit cell (yellow rectangle) seen in (a) is also indicated in (b) revealing that in (a) not all molecules are resolved. For details, see text. c) HIM image of a large area TPC CNM suspended over a TEM grid covered with a thin carbon film. Underlying Cu grid is seen on the right corners.

TPC and transferred onto a holey microscopy grid (Quantifoil, Jena). The imaging contrast is highlighted by the two dark circular holes at the bottom of the micrograph which, resembling  $\infty$ , result from a rupture of the CNM. Otherwise, the material appears to preserve its mechanical integrity over the rest of the support, indicating a great fraction of laterally interconnected molecules. It is clear that individual molecules comprising the primary monolayer (Figure 2a,b) have undergone substantial chemical transformations to maintain a continuous two-dimensional character of the suspended sheet on such a large scale.

IRRAS and XPS were employed to follow changes in structure and chemical composition of the TPC SAM upon irradiation. The vibrational spectra displayed in Figure 3a reveal pronounced changes upon irradiation with the complete disappearance of the most intense band at 1406 cm<sup>-1</sup> as the most striking difference. Attributed to the symmetric stretching of the bidentate COO<sup>-</sup> anchor group,<sup>[20]</sup> this suggests either a profound chemical change or a complete loss of the carboxylate moiety. Furthermore, the bands located in the region 1485 to 1605 cm<sup>-1</sup> and around 3000 cm<sup>-1</sup>, assigned to the skeletal and C–H stretching modes of the terphenyl moiety,

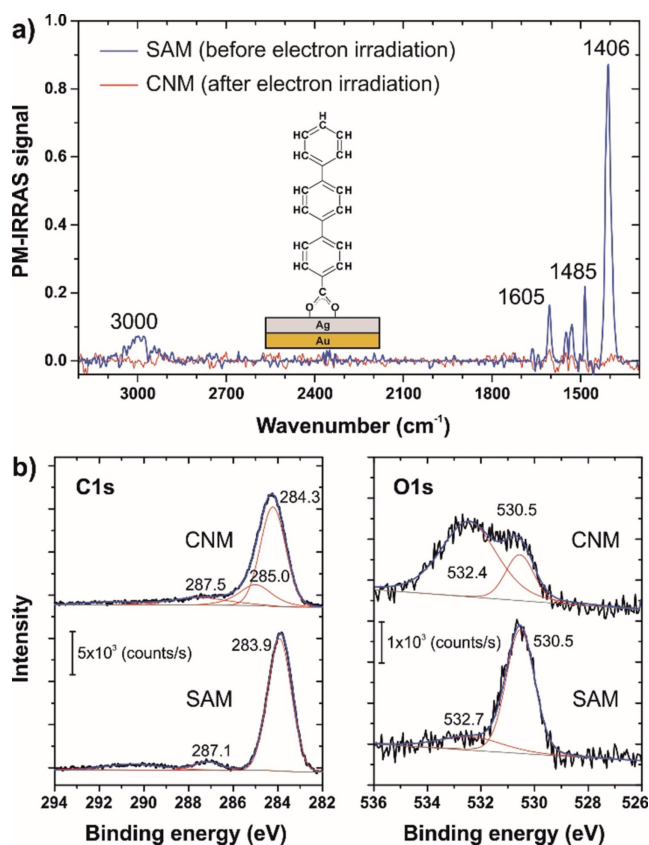


**Figure 3.** IRRAS (a) and XPS (b) spectra of pristine and cross-linked TPC SAM on Ag/Au/mica. The irradiated samples were exposed to air prior to taking spectra.

respectively, are similarly affected.<sup>[10]</sup> Their vanishing intensity after irradiation indicates fundamental changes in the geometrical arrangement of the molecular moieties and chemical nature of the layer as can be expected from cross-linking of the molecules.

Comparing the XP spectra before and after irradiation (Figure 3b), both the C1s and O1s regions show clear differences. The main peak in the C1s spectrum shifts to higher binding energy and is broadened, which, in agreement with the IRRAS data, reflects a chemical change of the terphenyl moieties. Chemical changes give also rise to intensity in the region between 285–287 eV and, as a consequence, it is not really possible to infer on changes of the carboxylate signal which is clearly visible in the native SAM at 287.1 eV. Even though there are significant changes in the C 1 s signal, its overall intensity is not altered substantially, which is in agreement with previous work on thiol based aromatic SAMs<sup>[10]</sup> and indicates that, despite pronounced chemical changes, not much material is lost.

In the O1s region electron irradiation causes major changes. The native layer is characterized by the carboxylate signal at 530.5 eV.<sup>[18]</sup> A minor signal at 532.7 eV indicates the presence of additional species which is ascribed to some oxygen containing carbon, observed when the SAMs are exposed to ambient atmosphere. Irradiation results in a significant reduction of the

oxygen signal of surface-bound carboxylate groups whereas a large and broad signal at around 532.4 eV evolves. This feature is assigned to dangling carbonyl and/or carboxylate groups, i.e. with oxygen atoms not directly connected to the substrate.<sup>[21]</sup> It is noted that the gain of this signal upon irradiation is significantly larger than the loss of the one at 530.5 eV which makes it difficult to explain this gain just by a conversion of the carboxylate moiety. Considering that the sample is exposed to atmosphere after irradiation, it is more likely that unstable species, generated by the electron bombardment under vacuum, react with oxygen and water vapor. This is in agreement with the C1s signal where the changes are too large to be explained by changes of the small carboxylate signal.

While the IRRAS and XPS data, in general, are consistent, there is one open point at this stage which has to be investigated further. The IRRAS data show a complete disappearance of the band at 1406 cm<sup>-1</sup> and possible interpretations are a complete elimination of the carboxylate moiety, a distinct chemical change, reorientation, or a combination of all three. The XPS O1s signal seems to contradict the complete elimination as a significant carboxylate signal is still observed after irradiation. However, since oxygen species adsorbed on Ag also generate a signal in the 530.5 eV region,<sup>[22]</sup> the difference between the IRRAS and XPS data for the carboxylate remains elusive. In this context it is worth noting that the study of biphenyl SAMs on thick Ag films reported an essentially complete loss of the carboxylate O1s signal, even though the structure of the SAMs differs from the purely aromatic TPC SAM by a short aliphatic chain between the carboxylate and the aromatic moiety.<sup>[11]</sup>

## 2.2. Functional Characterization

Irrespective of the incomplete knowledge of the chemical composition and mechanistic details, the generation of the free-standing TPC membranes was reliable. Six intact micrometer-sized samples were studied with respect to gas and vapor permeation. Figure 4 illustrates transport rates of several pure substances. The permeance  $\Pi$  was measured with a mass spectrometer as following:<sup>[15]</sup>

$$\Pi = \frac{J}{A \times p} \quad (1)$$

where  $J$  is the molar flow rate through the membrane,  $A$  is the membrane area, and  $p$  is the applied feed pressure.

Similar to TPT CNMs, the material exhibits high affinity to water vapor with a pronounced humidity dependence. This behavior was recently rationalized in terms of water condensation and collective motion of hydrogen-bonded molecules when the mass transfer is determined by surface species rather than gas-phase ones.<sup>[13,15]</sup> On the contrary, the passage of inert gas particles is significantly hindered, and only helium flow could be detected. The phenomenon is believed to be caused by a tortuous nature of the transmembrane channels, which imposes steric barriers for gaseous species.<sup>[16]</sup> Similar to water

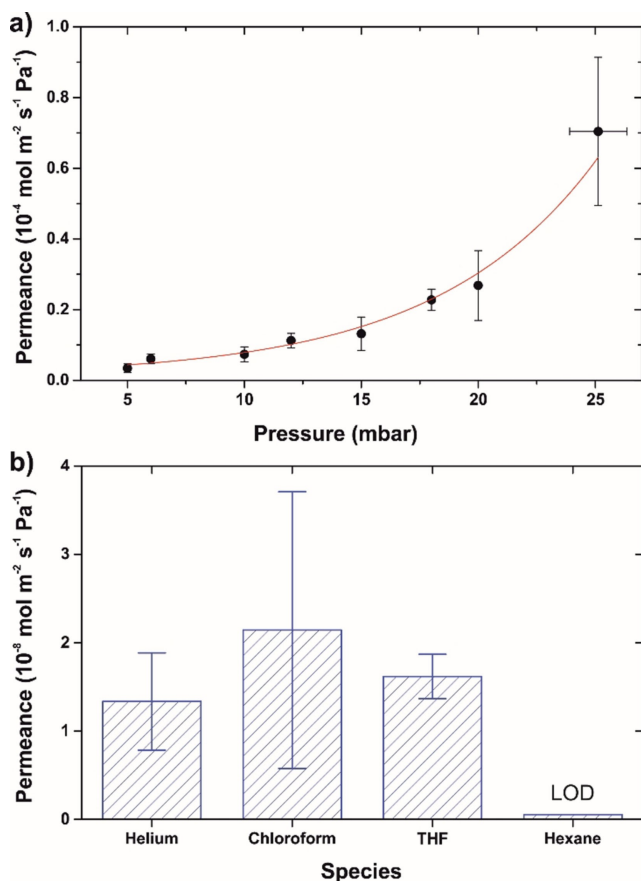


**Figure 4.** a) Permeance of D<sub>2</sub>O vapor in TPC CNMs as a function of its pressure. The data represent mean values over 10 measurements with 6 different samples. Error bars are standard deviations. The last point at 25 mbar corresponds to the saturation vapor pressure, and it changed due to temperature fluctuations. The solid line is intended to guide the eye. b) Permeance of net species in TPC CNMs at the following feed pressures: p(He) = 250 mbar; p(CHCl<sub>3</sub>) ≈ 240 mbar (sat.); p(C<sub>4</sub>H<sub>8</sub>O) ≈ 200 mbar (sat.); p(C<sub>6</sub>H<sub>14</sub>) ≈ 180 mbar (sat.). The data were averaged over multiple room-temperature measurements with 6 samples. LOD is the limit of detection as specified in ref. 15.

though, saturated organic vapors are expected to adsorb and diffuse on the membrane surface, and indeed, small permeation rates were obtained for chloroform and tetrahydrofuran (THF). In fact, despite the difference in the molecular sizes, the fluxes measured are comparable to that of helium, and the explanation is the different transport mechanisms. While only direct impact translocation is possible for helium atoms, adsorption-mediated permeation is likely to take place for solvent molecules.<sup>[17]</sup> However, surface diffusion was not observed for bulkier hexane molecules which is very much analogous to TPT CNMs.<sup>[16]</sup> In general, our mass transfer measurements revealed no essential difference between TPC and TPT nanomembranes, suggesting their similar microstructure. The head groups seem to play no significant role in the carbonization process, as long as the molecular backbone and the packing density do not differ much.

Although the observed permselectivity (Figure 4) looks promising for separating water-organic mixtures, it is a so called

ideal gas value and should be controlled in experiments with mixtures. THF is a versatile solvent which forms a minimum boiling homogenous azeotrope with water at 64 °C and atmospheric pressure.<sup>[23]</sup> To produce anhydrous THF, extractive distillation with various entrainers is usually employed, whereas dehydration with membranes is considered to be more energy-efficient.<sup>[24]</sup> In this work, we performed vapor permeation experiments with TPC CNMs exposed to water-THF mixtures. One-to-one feed composition was achieved by introducing saturated D<sub>2</sub>O vapor into 25 mbar vaporous THF, as described in the earlier publication.<sup>[16]</sup> Under such model conditions, the membrane selectivity was found to amount to at least 500 (with respect to the mass-spectrometer detection limit). Very similar performance was noticed for TPT CNMs, confirming again the same microporous nature of the carbonized material.

CNMs are known to be converted to graphene upon heating to 800 °C.<sup>[25]</sup> This is the reason why their atomic structure is difficult to resolve with electron microscopy, because beam heating induces further transformations during imaging. There exist many types of amorphous carbon allotropes, but it is well accepted that they are all categorized into either graphitizable or non-graphitizable.<sup>[26]</sup> The former ones are more ordered and able to continuously rearrange into graphitic structures with temperature. Both classes consist of irregular sheets of sp<sup>2</sup>-hybridized C atoms interconnected by sp<sup>3</sup> C atoms, and the difference is that the sp<sup>2</sup> regions in graphitizable materials are less cross-linked.

Indeed, the partial loss of aromaticity and appearance of aliphatic carbon in TPT SAMs was unambiguously revealed by high resolution electron energy loss spectroscopy (HREELS).<sup>[10c]</sup> The fact that CNMs readily yield graphene is indicative of the favorable orientation of their sp<sup>2</sup> constituents. Interestingly enough, the results of our gas and vapor permeation measurements evidenced a tortuous character for the membrane interior.<sup>[17]</sup> The only way to correlate these data with the earlier reported AFM images<sup>[13]</sup> is to assume that the interlaminar spacing in CNMs is the very bottleneck controlling their separation performance. Given the similarity between the nanomembranes made of TPC and TPT precursors, we propose that the radiation carbonization of aromatic SAMs obeys a generic mechanism. The surface mediation seems to facilitate the reorganization preferentially in the plane direction, giving rise to the laminar microstructure. Moreover, the length of the backbone of the SAM molecules is likely to determine the strength of the final material as the lateral integrity depends on the vertical cross-linking. Consequently, shorter components derived from biphenyl, such as biphenylthiol (BPT) and nitro-biphenylthiol (NBPT), were found to be much less suitable for producing defect-free micrometer-sized membranes, featuring irregular nanoscale holes.<sup>[27]</sup>

### 3. Conclusion

We showed that carboxylate SAMs on electrodeposited silver could be easily converted into functional nanomembranes. For the first time, the ultrasensitive permeation apparatus was

applied to compare molecular transport in free-standing CNMs prepared from different head groups and on different substrates. The results obtained revealed very similar characteristics over TPC and TPT membranes, indicating common structural motifs of the carbonaceous materials. Electron irradiation of the densely packed adsorbates was proven to be an effective method for producing nanometer-thick microporous films. The chemical separation with CNMs displayed a narrow size distribution of their ducts, suggesting a somewhat higher degree of ordering in the transverse direction compared to the lateral one.

This study further establishes carbonized polyaromatic SAMs as generic systems for permeable nanomembranes and, by demonstrating the suitability of aromatic carboxylic acids in combination with UPD-Ag substrates, substantially broadens the basis of molecular precursors. Extension beyond the standard combination, thiolates on gold, opens the possibility of a more flexible design of precursor layers enabling new architectures as recently demonstrated with SAMs featuring nanotunnels and the option of intercalating additional species.<sup>[28]</sup> Albeit carboxylate SAMs have been shown to form also on Ag films,<sup>[11]</sup> the use of UPD-Ag substrates offer a convenient handling of substrates as regards control of oxidation and contaminations. Firstly, the electrodeposition of Ag bilayer on Au enables the use of freshly prepared substrates that outperform commercial thin films in terms of surface cleanliness. Secondly, these substrates can be easily handled in air and even in aqueous environments. It is noted that the range of substrates can be further extended to Cu-UPD by employing the analogous electrodeposition procedure.<sup>[29]</sup> We anticipate that future developments exploring the structural and functional variability of aromatic carboxylic acids, also in combination with widespread metals like copper and aluminum enables the development towards large-area ultrathin separation membranes, thus, reinforcing the application prospects of CNMs.

## Experimental Section

### SAMs and CNMs Preparation

Epitaxial gold substrates on mica (Georg Albert PVD) were used for both TPC and TPT systems. TPC SAMs were prepared with *p*-(terphenyl)-4-carboxylic acid (97% Aldrich) dissolved in 50/50 (vol.) water-ethanol mixture (saturated solution at room temperature). Prior to silver deposition, Au/mica was flame annealed and immersed into 10 mM AgNO<sub>3</sub> solution in 100 mM HNO<sub>3</sub>. After a potential of 10 mV was applied for 2 min, the substrates were immediately placed into the preheated TPC solution and left overnight at 65 °C. The incubation time was around 20 hours. The substrates were then rinsed with ethanol and blown dry with N<sub>2</sub>. The preparation of TPT SAMs was done with sublimated *p*-(terphenyl)-4-thiol (97%, Sigma-Aldrich) dissolved in anhydrous N,N-dimethylformamide (99.8%, Sigma-Aldrich). In this case Au/mica as delivered was first cleaned with ozone and subsequently outgassed in vacuum. Assembly was over 24 hours at 75 °C under argon atmosphere using a 100 nM TPT solution. The substrates were rinsed with DMF and ethanol and blown dry with N<sub>2</sub>.

SAMs samples were loaded into a homemade radiation chamber and evacuated down to  $5 \times 10^{-8}$  mbar. An electron flood gun with beam energy of 100 eV was employed to irradiate the substrates for 12 min, and the total exposure corresponded to 50 mC/cm<sup>2</sup>. CNMs on native substrates were covered with poly(methyl methacrylate) (PMMA) by means of a spin coater and dried on a hot plate at 90 °C. The benzene solutions of 50 and 950 kDa PMMA were used to deposit two protection layers respectively. Afterwards, mica was detached and gold was etched away in an aqueous I<sub>2</sub>/KI solution. No additional etching step was undertaken for the Ag covered substrates. CNMs with PMMA were thoroughly rinsed in ultrapure water and transferred onto either Quantifoil Multi A TEM grids (Quantifoil Micro Tools GmbH) for helium ion microscopy or perforated Si<sub>3</sub>N<sub>4</sub>/Si windows (Silson Ltd) for permeation measurements. The size of the suspended CNMs samples varied between 2 and 7 micrometers.

### STM and HIM Measurements

STM imaging was performed with a Molecular Imaging Pico IS microscope under ambient conditions. A Pt/Ir 80:20 wire (Advent Research Materials Ltd., 0.25 mm diameter) was used to cut tips mechanically. Tunneling parameters were typically between 0.010–0.070 nA, and  $\pm 0.20$ –0.60 V.

Free-standing nanomembranes were imaged with a helium ion microscope (Zeiss Orion Plus) at a resolution limit below 1 nm. The images were scanned at 1  $\mu$ s dwell time, beam energy of 35 keV, and a beam current of 0.3 pA.

### IRRAS and XPS Measurements

IRRAS spectra were taken at a spectrometer VERTEX 70 (Bruker) equipped with a polarization-modulated reflectance module PMA 50 (Bruker). During measurements, the spectrometer was purged with a dry nitrogen flow of 3 L/min. The MCT detector was cooled with liquid nitrogen. Typically, 1024 scans were recorded at resolution of 4 cm<sup>-1</sup>.

XPS spectra were obtained in an ultrahigh vacuum ( $10^{-11}$  mbar) Multiprobe system (Omicron) with a monochromatic X-ray source (Al K <sub>$\alpha$</sub> , 1486.7 eV) and a hemispherical electron analyzer (SPHERA) with pass energy of 25 eV. The binding energy scale was calibrated relative to Au 4f<sub>7/2</sub> peak at 84.0 eV. The data were evaluated with CasaXPS software. The spectra were fitted by a sum of Gaussian/Lorentzian functions using linear backgrounds.

### Permeation Measurements

Mass transfer measurements with free-standing CNMs were carried out at the custom-made system described in [15]. Briefly, a suspended CNM sample was secured between a high vacuum detection chamber with a quadrupole mass-spectrometer and a multi-section feed compartment. Steady-state permeation rates were determined upon exposing CNMs to defined amounts of gaseous and vaporous substances as measured with a capacitance manometer. Helium was supplied by Linde. Chloroform (VWR, 99.8%), tetrahydrofuran (Fisher Chemical, 99.99%), hexane (Fisher Scientific, 95%), and heavy water (Sigma-Aldrich, 99.9% atom D) were repeatedly degassed before use.

## Acknowledgements

P. D. thanks the "Fonds der Chemischen Industrie" for a Liebig Fellowship, the Royal Society of Chemistry for a Researcher Mobility Grant, and the "Max-Buchner-Forschungstiftung" for a Max-Buchner Fellowship. P. D. is also grateful to Kelly Turner and Zhen Yao for their kind assistance during his stay in St Andrews. This work was in part financed by the German Federal Ministry for Education and Research (BMBF) within the bilateral German-Greek Research and Innovation Cooperation, project Caerus 03XP0155 A.

## Conflict of Interest

The authors declare no conflict of interest.

**Keywords:** amorphous materials · membranes · self-assembly · thin films · vapor permeation

- [1] H. B. Park, J. Kamcev, L. M. Robeson, M. Elimelech, B. D. Freeman, *Science* **2017**, *356*, eaab0530.
- [2] a) B. Zornoza, B. Seoane, J. M. Zamaro, C. Téllez, J. Coronas, *ChemPhysChem* **2011**, *12*, 2781–2785; b) T. M. Osborn Popp, A. Z. Plantz, O. M. Yaghi, J. A. Reimer, *ChemPhysChem* **2020**, *21*, 32–35; c) G. He, M. Dakhchoune, J. Zhao, S. Huang, K. V. Agrawal, *Adv. Funct. Mater.* **2018**, *1707427*; d) A. Knebel, P. Wulfert-Holzmann, S. Friebe, J. Pavel, I. Strauß, A. Mundstock, F. Steinbach, J. Caro, *Chem. Eur. J.* **2018**, *24*, 5728–5733; e) R. L. Papurello, L. A. Lozano, E. V. Ramos-Fernández, J. L. Fernández, J. M. Zamaro, *ChemPhysChem* **2019**, *20*, 3201–3209; f) Y. Peng, Y. Li, Y. Ban, W. Yang, *Angew. Chem. Int. Ed.* **2017**, *56*, 9757–9761.
- [3] a) B. P. Biswal, H. D. Chaudhari, R. Banerjee, U. K. Kharul, *Chem. Eur. J.* **2016**, *22*, 4695–4699; b) V. A. Kuehl, J. Yin, P. H. H. Duong, B. Mastorovich, B. Newell, K. Li-Oakley, B. A. Parkinson, J. O. Hoberg, *J. Am. Chem. Soc.* **2018**, *140*, 18200–18207; c) K. Dey, M. Pal, K. C. Rout, H. S. Kunjattu, A. Das, R. Mukherjee, U. K. Kharul, R. Banerjee, *J. Am. Chem. Soc.* **2017**, *139*, 13083–13091; d) M. Shan, B. Seoane, E. Rozhko, A. Dikhtiarenko, G. Clet, F. Kapteijn, J. Gascon, *Chem. Eur. J.* **2016**, *22*, 14467–14470.
- [4] a) M. Y. Jeon, D. Kim, P. Kumar, P. S. Lee, N. Rangnekar, P. Bai, M. Shete, B. Elyassi, H. S. Lee, K. Narasimharao, S. N. Basahel, S. Al-Thabaiti, W. Xu, H. J. Cho, E. O. Fetisov, R. Thyagarajan, R. F. DeJaco, W. Fan, K. A. Mkhoyan, J. I. Siepmann, M. Tsapatsis, *Nature* **2017**, *543*, 690–694; b) D. Kim, M. Y. Jeon, B. L. Stottrup, M. Tsapatsis, *Angew. Chem. Int. Ed.* **2018**, *57*, 480–485; c) Z. Cao, S. Zeng, Z. Xu, A. Arvanitis, S. Yang, X. Gu, J. Dong, *Sci. Adv.* **2018**, *4*, eaau8634; d) T. H. Nguyen, H. Gong, S. S. Lee, T. H. Bae, *ChemPhysChem* **2016**, *17*, 3165–3169.
- [5] a) H. Richter, H. Voss, N. Kaltenborn, S. Kämnitz, A. Wollbrink, A. Feldhoff, J. Caro, S. Roitsch, I. Voigt, *Angew. Chem. Int. Ed.* **2017**, *56*, 7760–7763; b) C. Zhang, W. J. Koros, *Adv. Mater.* **2017**, *29*, 1701631; c) D. Bouša, K. Friess, K. Pilnáček, O. Vopička, M. Lanč, K. Fónod, M. Pumera, D. Sedmidubský, J. Luxa, Z. Sofer, *Chem. Eur. J.* **2017**, *23*, 11416–11422; d) P. Panigrahi, A. K. Dhinakaran, Y. Sekar, R. Ahuja, T. Hussain, *ChemPhysChem* **2018**, *19*, 2250–2257.
- [6] A. Turchanin, A. Götzhäuser, *Adv. Mater.* **2016**, *28*, 6075–6103.
- [7] J. C. Love, L. A. Estroff, J. K. Kriebel, R. G. Nuzzo, G. M. Whitesides, *Chem. Rev.* **2005**, *105*, 1103–1170.
- [8] P. Angelova, H. Vieker, N.-E. Weber, D. Matei, O. Reimer, I. Meier, S. Kurasch, J. Biskupek, D. Lorbach, K. Wunderlich, L. Chen, A. Terfort, M. Klapper, K. Müllen, U. Kaiser, A. Götzhäuser, A. Turchanin, *ACS Nano* **2013**, *7*, 6489–6497.
- [9] a) X. Zhang, C. Neumann, P. Angelova, A. Beyer, A. Götzhäuser, *Langmuir* **2014**, *30*, 8221–8227; b) P. Penner, X. Zhang, E. Marschewski, F. Behler, P. Angelova, A. Beyer, J. Christoffers, A. Götzhäuser, *J. Phys. Chem. C* **2014**, *118*, 21687–21694; c) C. Yildirim, E. Sauter, A. Terfort, M. Zharnikov, *J. Phys. Chem. C* **2017**, *121*, 7355–7364.
- [10] a) W. Eck, A. Küller, M. Grunze, B. Völkel, A. Götzhäuser, *Adv. Mater.* **2005**, *17*, 2583–2587; b) A. Turchanin, D. Käfer, M. El-Desawy, C. Wöll, G. Witte, A. Götzhäuser, *Langmuir* **2009**, *25*, 7342–7352; c) L. Amiaud, J. Houplin, M. Bourdier, V. Humblot, R. Azria, C.-M. Pradier, A. Lafosse, *Phys. Chem. Chem. Phys.* **2014**, *16*, 1050–1059; d) J. Houplin, C. Dablemont, L. Sala, A. Lafosse, L. Amiaud, *Langmuir* **2015**, *31*, 13528–13534; e) C. Yildirim, M. Füser, A. Terfort, M. Zharnikov, *J. Phys. Chem. C* **2017**, *121*, 567–576.
- [11] C. Neumann, M. Szwed, M. Frey, Z. Tang, K. Koziel, P. Cyganik, A. Turchanin, *ACS Appl. Mater. Interfaces* **2019**, *11*, 31176–31181.
- [12] G. Capozzi, G. Modena, in *The Chemistry of the Thiol Group, Part 2* (Ed.: S. Patai), John Wiley&Sons Ltd., **1974**, pp. 785–839.
- [13] Y. Yang, P. Dementyev, N. Biere, D. Emmrich, P. Stohmann, R. Korzetz, X. Zhang, A. Beyer, S. Koch, D. Anselmetti, A. Götzhäuser, *ACS Nano* **2018**, *12*, 4695–4701.
- [14] Y. Yang, R. Hillmann, Y. Qi, R. Korzetz, N. Biere, D. Emmrich, M. Westphal, B. Büker, A. Hütten, A. Beyer, D. Anselmetti, A. Götzhäuser, *Adv. Mater.* **2020**, 1907850.
- [15] P. Dementyev, T. Wilke, D. Naberezhnyi, D. Emmrich, A. Götzhäuser, *Phys. Chem. Chem. Phys.* **2019**, *21*, 15471–15477.
- [16] D. Naberezhnyi, A. Götzhäuser, P. Dementyev, *J. Phys. Chem. Lett.* **2019**, *10*, 5598–5601.
- [17] P. Dementyev, Y. Yang, M. Rezvova, A. Götzhäuser, *J. Phys. Chem. Lett.* **2020**, *11*, 238–242.
- [18] H. Aitchison, H. Lu, S. W. L. Hogan, H. Früchtel, I. Cebula, M. Zharnikov, M. Buck, *Langmuir* **2016**, *32*, 9397–9409.
- [19] a) V. V. Korolkov, S. Allen, C. J. Roberts, S. J. B. Tandler, *J. Phys. Chem. C* **2011**, *115*, 14899–14906; b) A. Bashir, W. Azzam, M. Rohwerder, A. Terfort, *Langmuir* **2013**, *29*, 13449–13456.
- [20] a) N. E. Schlotter, M. D. Porter, T. B. Bright, D. L. Allara, *Chem. Phys. Lett.* **1986**, *132*, 93–98; b) E. L. Smith, M. D. Porter, *J. Phys. Chem.* **1993**, *97*, 8032–8038; c) A. Krzykawska, J. Ossowski, T. Zaba, P. Cyganik, *Chem. Commun.* **2017**, *53*, 5748–5751; d) M. H. Hsu, W. S. Hu, J. J. Lin, Y. J. Hsu, D. H. Wei, C. W. Yang, C. S. Chang, Y. T. Tao, *Langmuir* **2004**, *20*, 3641–3647.
- [21] a) S. Stepanow, T. Strunskus, M. Lingenfelder, A. Dmitriev, H. Spillmann, N. Lin, J. V. Barth, Ch. Wöll, K. Kern, *J. Phys. Chem. B* **2004**, *108*, 19392–19397; b) W. Zhang, A. Nefedov, M. Naboka, L. Cao, Ch. Wöll, *Phys. Chem. Chem. Phys.* **2012**, *14*, 10125–10131.
- [22] T. C. R. Rocha, A. Oestereich, D. V. Demidov, M. Hävecker, S. Zafeiratos, G. Weinberg, V. I. Bukhtiyarov, A. Knop-Gericke, R. Schlögl, *Phys. Chem. Chem. Phys.* **2012**, *14*, 4554–4564.
- [23] Z. Zhang, D. Huang, M. Lv, P. Jia, D. Sun, W. Li, *Sep. Purif. Technol.* **2014**, *122*, 73–77.
- [24] L. M. Vane, *J. Chem. Technol. Biotechnol.* **2019**, *94*, 343–365.
- [25] D. G. Matei, N.-E. Weber, S. Kurasch, S. Wundrack, M. Woszczyna, M. Grothe, T. Weimann, F. Ahlers, R. Stosch, U. Kaiser, A. Turchanin, *Adv. Mater.* **2013**, *25*, 4146–4151.
- [26] E. H. L. Falcao, F. Wudl, *J. Chem. Technol. Biotechnol.* **2007**, *82*, 524–531.
- [27] Unpublished data.
- [28] R. Ortiz de la Morena, A. Asyuda, H. Lu, H. Aitchison, K. Turner, S. M. Francis, M. Zharnikov, M. Buck, *Phys. Chem. Chem. Phys.* **2020**, *22*, 4205–4215.
- [29] a) I. Cebula, C. Shen, M. Buck, *Angew. Chem. Int. Ed.* **2010**, *49*, 6220–6223; b) H. Aitchison, H. Lu, M. Zharnikov, M. Buck, *J. Phys. Chem. C* **2015**, *119*, 14114–14125; c) H. Aitchison, H. Lu, R. Ortiz de la Morena, I. Cebula, M. Zharnikov, M. Buck, *Phys. Chem. Chem. Phys.* **2018**, *20*, 2731–2740.

Manuscript received: February 25, 2020

Revised manuscript received: March 19, 2020

Accepted manuscript online: March 23, 2020

Version of record online: April 14, 2020